PCCP

PAPER

View Article Online
View Journal | View Issue

Cite this: *Phys. Chem. Chem. Phys.*, 2015, **17**, 3820

Thermodynamic insights into the self-assembly of capped nanoparticles using molecular dynamic simulations†

André F. de Moura,*[a] Kalil Bernardino,[a] Cleocir J. Dalmaschio,[b] Edson R. Leite[a] and Nicholas A. Kotov[c]

Although the molecular modeling of self-assembling processes stands as a challenging research issue, there have been a number of breakthroughs in recent years. This report describes the use of large-scale molecular dynamics simulations with coarse grained models to study the spontaneous self-assembling of capped nanoparticles in chloroform suspension. A model system comprising 125 nanoparticles in chloroform evolved spontaneously from a regular array of independent nanoparticles to a single thread-like, ramified superstructure spanning the whole simulation box. The aggregation process proceeded by means of two complementary mechanisms, the first characterized by reactive collisions between monomers and oligomers, which were permanently trapped into the growing superstructure, and the second a slow structural reorganization of the nanoparticle packing. Altogether, these aggregation processes were over after *ca.* 0.6 μs and the system remained structurally and energetically stable until 1 μs. The thread-like structure closely resembles the TEM images of capped ZrO_2, but a better comparison with experimental results was obtained by the deposition of the suspension over a graphene solid substrate, followed by the complete solvent evaporation. The agreement between the main structural features from this simulation and those from the TEM experiment was excellent and validated the model system. In order to shed further light on the origins of the stable aggregation of the nanoparticles, the Gibbs energy of aggregation was computed, along with its enthalpy and entropy contributions, both in chloroform and in a vacuum. The thermodynamic parameters arising from the modeling are consistent with larger nanoparticles in chloroform due to the solvent-swelled organic layer and the overall effect of the solvent was the partial destabilization of the aggregated state as compared to the vacuum system. The modeling strategy has been proved effective and reliable to describe the self-assembling of capped nanoparticles, but we must acknowledge the fact that larger model systems and longer timescales will be necessary in future investigations in order to assess structural and dynamical information approaching the behavior of macroscopic systems.

Received 6th August 2014,
Accepted 15th December 2014

DOI: 10.1039/c4cp03519d

www.rsc.org/pccp

Introduction

The complexity of colloidal suspensions of nanoparticles (NPs) capable of self-organization and dynamic agglomeration has hierarchical character and their structural motifs may span several orders of magnitude in length. The characteristic times of the processes affecting self-assembly outcome(s) also range from vibrations of chemical bonds at the femtosecond to picosecond timescale to the coalescence processes that may last several days.[1] As with other systems with equally complex hierarchy, different computational approaches need to be considered depending on the specific length-scales and timescales that are relevant for the phenomena under investigation, ranging from *ab initio* quantum chemistry methods, describing the electronic structure of a single NP, to coarse grained and continuum models, describing collective, large-scale features, both structural and dynamical.[2] This was shown to be possible for understanding the mechanical behavior of biological and biomimetic materials under strain,[3] and it should be possible for the understanding of self-assembly behavior, too, but that

[a] *Departamento de Química, Centro de Ciências Exatas e de Tecnologia, Universidade Federal de São Carlos, Rodovia Washington Luiz km 235, CP 676, CEP 13565-905, São Carlos, SP, Brasil. E-mail: moura@ufscar.br*
[b] *Departamento de Ciências Naturais, Centro Universitário Norte do Espírito Santo, Universidade Federal do Espírito Santo, Rodovia BR-101 Norte - km 60, CEP 29932-540, São Mateus, ES, Brasil*
[c] *Chemical Engineering Department, BioInterfaces Institute, Materials Science Department, Biomedical Engineering Department, University of Michigan, 2300 Hayward, Ann Arbor, MI, 48109 USA*

† Electronic supplementary information (ESI) available: Movies depicting the spreading and evaporation of the NPs suspension are available. See DOI: 10.1039/c4cp03519d

may be difficult to achieve due to questions regarding the progressive coarse-graining of the models without the loss of essential features of the process[4] and the clarity about the chemical changes during the self-assembly of NPs.

In order to correctly describe the chemical environment around NPs in solution, most simulations rely on a suitable classical potential energy surface, which may be parameterized to reproduce either the structure or the interactions of the system of interest—preferably both, as we briefly survey below.

Single NPs in explicit solvent have been studied for both charged[5] and neutral NPs.[6] These model systems point out possible stabilization mechanisms for colloidal suspensions, *e.g.*, the formation of an electric double layer around charged NPs in aqueous solution or the solvent swollen structures formed by the organic coating in contact with good solvents. Both phenomena should contribute to the colloidal stabilization, but larger models including the interaction between NPs are mandatory for a proper description of the thermodynamic stability of these suspensions.

We must acknowledge the fact that simulations may become computationally demanding if multiple NPs and explicit solvent molecules are considered. This intrinsic limitation is more severe for MD simulations using atomistic force fields, due to the large number of interaction sites comprising the system, the long relaxation times that are expected for a typical colloidal suspension, and the short integration time step. The choice of coarse-grained (CG) force fields seems to be obvious for systems larger than 10 nm in length and timescales longer than 100 ns, because the number of interaction sites decreases and the integration time step simultaneously increases, allowing a 1000-fold faster integration of the equations of motion for a typical CG force field.

Although unusual, some fully atomistic, large-scale simulations of grafted NP self-assembling have been reported. For instance, Lane and Grest[7,8] studied the association of water-insoluble NPs at the water–vacuum interface, using the all-atom force field for a system with edge lengths above 30 nm and reaching timescales of 200 ns, which demanded a very large amount of computer time. The NPs were coated with the aliphatic chain terminated with either apolar CH_3 groups or polar COOH groups and were insoluble due to the length of the hydrophobic chains forming the coating. Both CH_3-terminated and COOH-terminated coatings led to the formation of stable 2D aggregates lying at the water interface. Interestingly, the aggregates were filamentous and irregular, with a more compact arrangement for the apolar NPs.

Although computationally more efficient, CG models must be used judiciously, as they most likely lack proper parameterization for the specific NP under investigation. For instance, Lee *et al.*[9] studied a NP–polymer composite using a CG force field that needed specific parameterization to ensure that the polymer model was representative of poly(3-hexylthiophene) structure and NP and nanorod (NR) interactions were representative of the TiO_2 anatase phase. The model systems ranged from 55 to 57 nm, and both NPs (2.5 nm in diameter) and NRs (10 nm long, 2 nm in diameter) remained dispersed in the polymeric matrix. The polymer crystallinity was larger around the NRs as compared to the NPs, probably due to the alignment of the polymer chains along the NRs.

Leekumjorn *et al.*[10] used the MARTINI CG force field,[11] to study the effect of solvent polarity on the packing of the organic molecules adsorbed on the NP surface. The model was a hollow fullerene-like NP with oleic acid molecules attached to each surface site, and the systems comprised up to 27 NPs immersed in solvents ranging from hexane to water. The parameters describing each solvent and the oleic acid tails have been adjusted to reproduce solubility properties of each component, and thus the modeling strategy should be regarded as reliable. The most important feature arising from the simulations was the colloidal stabilization of the NPs in hexane, toluene and benzene, and the coalescence in chloroform, acetone, ethanol and water. The solvents that stabilized the colloidal suspensions also swelled the organic capping, whereas those that caused the NPs to aggregate also caused the capping to shrink.

The proper description of colloidal stability of capped NPs must rely on either of two approaches (or preferably both): the computation of the free energy of association for a dimer of NPs and/or the equilibrium simulation of a large system for a long time to assess whether or not stable aggregates are formed.

Damasceno *et al.*[12] performed a large series of Monte Carlo simulations to investigate the self-organization patterns of 145 hard convex polyhedra. This might seem to be a drastic case of coarse-graining since the particles lack any attractive potential energy term, but the excluded volume plays an important role here, giving rise to many-body entropic forces, which are modulated by the packing efficiency of each polyhedron. These entropic forces may become directional and then result in an ordered solid phase, which is the case for the more symmetric polyhedra, whereas less symmetrical polyhedra tend to form glassy solids. Altogether, these simulations make a clear statement on the role played by the shape of the building blocks during the self-assembly of NPs, even in the absence of any mechanical driving force.

Lin *et al.*[13] studied CG model systems comprising 8 Au NPs coated with alkanethiol chains immersed in water. Chain lengths varied from 4 to 20 atoms, rendering all NPs hydrophobic and water-insoluble. The NPs with the shortest chain length yielded two different structural patterns for the aggregated state, one with all NPs forming one single spherical aggregate, and the other with all NPs forming a long thread, spanning the whole length of the simulation box. This thread-like structure was observed less often (in 2 out of 10 independent simulations) and due to the periodic boundary conditions it behaved as an infinite linear aggregate.

The relation between colloidal stability and the swelling of the organic layer adsorbed on the NPs surface has been recently described by Dalmaschio *et al.*[14] for ZrO_2 NPs in either hexane or chloroform, using both experiments and computer modeling. The model NPs had nearly spherical cores and surface sites were completely covered by oleic acid molecules with the polar heads pointing to the NP surface. The NPs remained stable in hexane solution but aggregated in chloroform, which is consistent with

the experimental evidence, and the MD simulation presented an interesting microscopic picture, confirming that the organic layer became solvent-swollen in hexane and that organized layers of this solvent were built up around the NPs. This long-range order across the solvent may be thought of as a solvent mediated repulsion between NPs that ultimately renders them stable in hexane. On the other hand, the NPs became less swollen in chloroform and the solvent became less structured around the NPs, which is consistent with a solvent-induced attraction (solvent depletion between NPs).

The direct computation of the free energy changes involved in the association of NP dimers has been undertaken by a number of investigators. Sun *et al.*[15] have studied the association of a pair of passivated gold NPs in supercritical CO_2. This is the continuation of a previous investigation by Yang *et al.*[16] on the solubility of a single passivated NP in this solvent, which addressed a fundamental issue regarding the stability of this colloidal system, since individual NPs need to be soluble in the first place before any discussion regarding the way they interact with each other. As regards single NP solubility, lower solvent density increases the solubility whereas the length of the passivating chains may either increase the solubility at lower solvent density or decrease it at higher densities. In all cases that have been considered by Yang *et al.*[16] the energy contribution always favored the NP solubility in supercritical CO_2 while the entropic contribution was always unfavorable, pointing to a compromise between energy and entropy factors to describe the NP solubility.

The interaction between two passivated NPs in supercritical CO_2 was thoroughly studied by Sun *et al.*[15] by means of potential of mean force (PMF) profiles. The solvent destabilized the dimers as compared to vacuum and the degree of destabilization increased with the chain length. The thermodynamic potentials were further split into contributions arising from the cores and the self-assembled monolayers (SAMs) on the NP surface and it was demonstrated that direct core–core and core–solvent interactions were negligible as compared to SAM–SAM and SAM–solvent contributions. SAM–SAM interactions tended to stabilize the aggregated dimers while SAM–solvent contributions were mostly repulsive and changed in a complex way in response to the solvent density. The PMF profiles were also decomposed into direct and induced interactions and this analysis is consistent with free energy of association arising from a competition between direct and induced interactions. The direct term presented a favorable energy interaction, whereas its entropy contribution was unfavorable, mostly due to the steric hindrance between the tethered chains. Interestingly, the induced free energy had a favorable entropy change along with an unfavorable energy change for the NP association. This energy penalty was ascribed to the decreased interaction between the SAM chains and the solvent in the associated state as compared to the dissociated state. Some attractive energy contribution for the solvent–solvent interaction was observed as well at short distances for the systems with higher solvent density, which may be ascribed to the interaction involving solvent molecules which were within the SAM regions and were expelled upon association of the nanoparticles.

The present investigation is aimed at providing a thorough description of the association of the capped NPs recently described by Dalmaschio *et al.*[14] combining large-scale MD simulations and transmission electron microscope (TEM) images. The stable colloidal dispersion in hexane will not be considered here, since this system has already been properly described. On the other hand, the behavior of the NPs in chloroform needs further investigation to clarify both the kinetics and the thermodynamics of the aggregation process. From the standpoint of MD simulations, three approaches have been considered: (i) the spontaneous self-assembling of NPs in chloroform, (ii) the deposition of the colloidal suspension on a solid substrate and the solvent evaporation to form a thin film of NPs to be compared with the TEM images of NPs deposited on a carbon grid, and (iii) the estimation of the Gibbs energy of aggregation for a pair of NPs in either chloroform or a vacuum, along with its enthalpic and entropic contributions. Altogether, these simulations and the TEM images provided a detailed picture of the self-assembling process and the roles that might be played by the solvent.

Methodology

TEM images

The synthesis and characterization of the ZrO_2 NPs have been described elsewhere.[14] Samples were prepared by immersion of a 300-mesh carbon-coated copper grid in the chloroform suspension. The TEM/HRTEM images were obtained using a FEI TECNAI G2 F20 microscope operating at 200 kV.

MD simulations

The model systems were described using the MARTINI CG force field,[11] which is known to yield reasonable solubility properties for organic molecules in general, but on the other hand, lacks proper parameters for inorganic NPs. Although a bare NP cannot be accurately described by this force field, a capped NP may be conveniently treated if the capping layer is thick enough and compact enough to ensure that NPs interact with each other and with the solvent mostly through the organic layer on their surfaces.[15] Bearing these requisites in mind, we have drawn a model NP comprising a nearly spherical, crystalline core (d = 4 nm, simple cubic lattice and 0.35 nm between nearest neighbors sites) and 246 oleic acid molecules bonded to the surface sites (Fig. 1a).

The masses of the CG sites comprising the NP core were adjusted to yield the expected overall mass for a ZrO_2 NP with the same size and shape, in order to ensure the proper description of the translational and rotational dynamics of the NP. Altogether, each NP consisted of 2435 CG interaction sites, which were bonded to each other by means of quadratic harmonic potentials (force constants k_{bond} = 1250 kJ mol^{-1} nm^{-2} for oleic acid molecules and k_{bond} = 2500 kJ mol^{-1} nm^{-2} for the NP core). The oleic acid tails were attached to the surface sites by means of harmonic potentials as well (k_{bond} = 1250 kJ mol^{-1} nm^{-2}) and the slightly bent structure of each oleic acid tail was ensured by a set of quadratic harmonic angle potentials (cosine type),

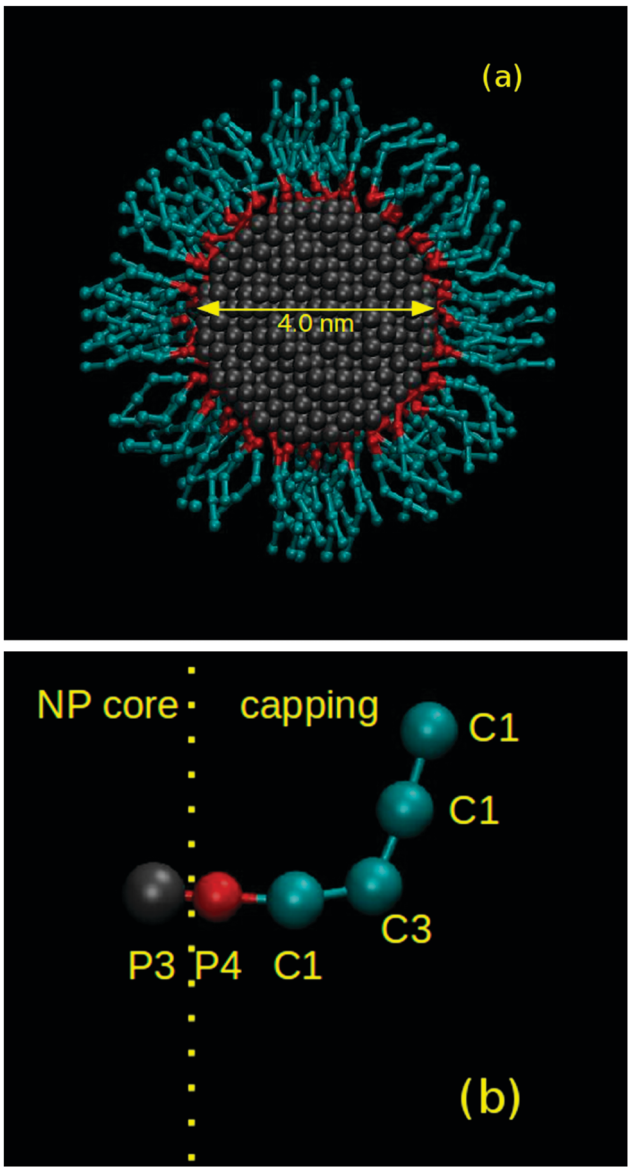

Fig. 1 (a) Graphical representation of the NP cross section. The NP core is 4.0 nm wide (dark gray sites) and the surface is completely covered by a dense monolayer of oleic acid molecules (polar heads are shown in red, whereas the apolar tail sites are shown in gray). (b) Type of interaction for each site comprising the NP core and the organic capping.

with $\theta_0 = 180^\circ$ and $k_{angle} = 25$ kJ mol^{-1} for three consecutive interaction sites forming a straight segment and $\theta_0 = 120^\circ$ and $k_{angle} = 45$ kJ mol^{-1} for the three consecutive interaction sites forming the *cis* defect. Besides these bonding interactions, each CG site interacted with other neighboring sites by means of a Lennard-Jones potential (eqn (1)), which may be classified as a soft sphere interaction between two sites, with no directional contribution.

$$V_{LJ}(r) = 4\varepsilon_{ij}\left[\left(\frac{\sigma_{ij}}{r_{ij}}\right)^{12} - \left(\frac{\sigma_{ij}}{r_{ij}}\right)^{6}\right] \quad (1)$$

The Lennard-Jones potential for a pair of particles i and j depends on two parameters, one describing the size of the particles (σ_{ij}) and the other being a measure of how strongly these particles may interact with each other (ε_{ij}). The MARTINI CG force field sets all σ_{ij} parameters to 0.47 nm, except for ring-like molecules (which are not present in our model system), so the only difference between the sites described in Fig. 1 is the depth of the potential well ε_{ij} between each pair of interacting particles (Table 1).

Table 1 Lennard-Jones parameters for the NP sites and the solvent. The sites are named according to the representation in Fig. 1

Interaction	Description/parameters	σ_{ij} (nm)	ε_{ij} (kJ mol^{-1})
Type 1	Polar head–polar head (P4–P4) NP core–NP core (P3–P3) Polar head–NP core (P4–P3)	0.47	5.0
Type 2	Apolar tail–apolar tail (C1–C1) Apolar tail–apolar tail (C1–C3) Apolar tail–apolar tail (C3–C3) Apolar tail–solvent (C3–C4) Solvent–solvent (C4–C4)	0.47	3.5
Type 3	Apolar tail–solvent (C1–C4) NP core–solvent (P3–C4) NP core–apolar tail (P3–C4)	0.47	3.1
Type 4	Polar head–solvent (P4–C4) Polar head–apolar tail (P4–C3)	0.47	2.7
Type 5	NP core–apolar tail (P3–C1)	0.47	2.3
Type 6	Polar head–apolar tail (P4–C1)	0.47	2.0

The non-bonded interactions were cutoff at 1.2 nm along with a shift function for separation distances between 0.9 and 1.2 nm to damp the noise that would be otherwise formed due to the force discontinuity at the cut-off distance. As regards the choice of parameters, the NP core should be considered as made up of moderately polar units (type P3), whereas the oleic acid molecules are described by the polar parameters for the head site (type P4) and two different apolar parameters sets for the tails sites, belonging either to type C3 (site bearing the double bond/*cis* defect) or to the type C1 (saturated sites/linear chain). One word of caution is necessary here, regarding the polar and apolar classifications for the MARTINI parameters, which should be used with care, since these terms mean that those molecules and molecular fragments present solubility properties that resemble actual polar and apolar species, respectively. The interaction sites do not bear charge dipoles and thus their force field description should not be taken literally.

Production runs were preceded by energy minimization runs using both steepest descent and conjugated gradient methods, in order to avoid strong repulsive contacts that might lend the trajectories unstable. The trajectories were integrated using the leapfrog algorithm with a time step ranging from 10 fs in a vacuum to 20 fs in solution, updating the neighbors list every ten integration steps. All the simulations and analyses were carried out using the GROMACS suite (version 4.5.5)[17,18] running on the Linux-based high performance computing cluster, FLUX, at the University of Michigan and on a Dell Poweredge R815 64-core, Linux-based server at the Federal University of São Carlos.

The graphical representations of the systems were rendered using the VMD for Linux (version 1.9.1).[19]

A concluding remark about the model system is that the range of all potential energy contributions is too short to be directly responsible for aggregation patterns spanning several nanometers. Besides being short-ranged, all pair interactions lack directional information. Thus, any oriented attachment pattern cannot be ascribed to the direct interactions between NPs and should then be ascribed to many-body effects, as will be discussed in the next section.

Spontaneous self-assembling in chloroform

The initial structure consisted of a regular $5 \times 5 \times 5$ NPs array in a cubic box with 55 nm of edge length (Fig. 2). The box was filled with chloroform molecules, which were modeled as a single CG interaction site (type C4), resulting in a model system with *ca.* 1.5 million interaction sites and a concentration $x = 0.0001$ for the NPs. Solvent and NPs were coupled to independent heat baths using the v-rescale algorithm[20] (T = 300 K and τ_T = 0.1 ps). The pressure was controlled using the weak-coupling scheme of Berendsen[21] (P = 1 bar, τ_P = 0.2 ps and $\kappa = 3 \times 10^{-5}$ bar^{-1}). The equations of motion were integrated up to 1 μs, but the MARTINI CG force field is known to produce artificially faster dynamics, so the actual timescale would probably be fourfold larger.[11]

NP deposition on a graphene surface

Structures arising from the MD simulation of the NP suspension cannot be directly compared with the results obtained using TEM, mostly because TEM produced 2-dimensional images of dry NPs over carbon-coated grids whereas MD simulations yielded 3-D patterns formed by solvated NPs. In order to overcome this intrinsic limitation, we devised a computational protocol to simulate the simultaneous deposition and evaporation of the suspension over a model carbon grid, yielding a 2-dimensional NP distribution that might be compared directly with the TEM images.

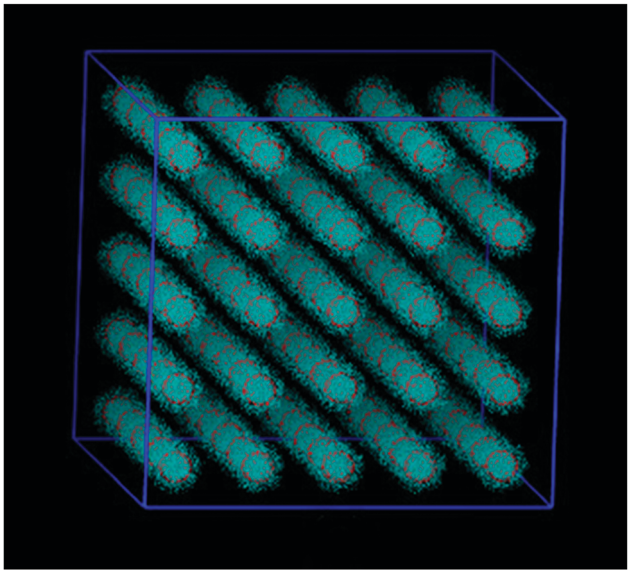

Fig. 2 Initial structure for the colloidal suspension model system. Solvent molecules are not shown for clarity.

The final structure from the MD simulation of NPs suspended in chloroform was placed at the center of a larger box, with edges 88.452, 88.41949 and 200.000 nm (all simulations were carried out at constant volume). At the bottom of this simulation box we placed an idealized carbon grid formed by a four-layer graphene substrate periodically replicated in the *xy*-plane. The substrate comprised 530 712 CG interaction sites, which were kept frozen during the simulations, each CG site corresponding to two carbon atoms. On the one hand, freezing solid substrate sites may help to speed up simulations, but on the other any perfectly crystalline solid surface may enhance an artifact which typically affects CG model systems, the freezing of liquid at the solid–liquid interface.[11] In order to avoid this artifact and to render the model system more realistic, we introduced some surface defects in the substrate, changing the Lennard-Jones parameters for 5% of the graphene sites from $\varepsilon = 2.7$ kJ mol^{-1} and $\sigma = 0.47$ nm to $\varepsilon = 2.3$ kJ mol^{-1} and $\sigma = 0.55$ nm. These randomly placed defects created sites which were simultaneously larger and weakly interacting and thus were less prone to induce solvent organization and freezing.

The first step of the protocol consisted of a 3.2 ns-long MD simulation at T = 300 K to allow the relaxation of the cubic structure taken from the end of the previous simulation into a spherical droplet (this is a spontaneous process due to the surface area decrease accompanying the change from a cube to sphere, resulting in an overall surface energy minimization). During this short period of time some chloroform spontaneously vaporized, as expected for this highly volatile solvent, filling the whole simulation box with a homogenous vapor in equilibrium with the suspension droplet. After equilibrium was attained, the second step of our protocol began, consisting of the forced deposition of the suspension droplet on the solid substrate. A harmonic potential with a force constant of 10^6 kJ mol^{-1} nm^{-2} was applied for the z-coordinate of the separation between the center of mass of the droplet and the surface of the solid substrate (the large force constant was necessary to induce the deposition within a reasonable amount of computer time). The pulling force was turned off when the droplet reached the substrate surface, after 7.85 ns of simulation.

The drying process was carried out at 320 K by the removal of solvent vapor that formed spontaneously from the liquid suspension. All solvent molecules with z-coordinate larger than 90 nm were removed every 0.1 ns, mimicking the effect of a vacuum pump placed at this position. Just like in an experimental setup, there cannot be liquid–vapor equilibrium since the molecules are irreversibly removed. In this sense, this model cannot be assigned to any statistical mechanics ensemble and the simulation is representative of a non-equilibrium process.

Gibbs energy of aggregation

The Gibbs energy profile along a specified path connecting two well-defined thermodynamic states of a system may be derived by the integration of the force averaged over an ensemble of configurations along the path, yielding the so-called potential

of mean force (PMF). The processes of interest for the present investigation are the association and the dissociation of a pair of NPs either in a vacuum or in chloroform and the path between the dissociated state and the associated state is simply a sequence of radial distances between the centers of mass of the NPs. If the separation between the NPs changes very slowly, the PMF profiles for both processes should be the same, whereas some degree of hysteresis might be observed for faster pulling rates. The presence of hysteresis should be ascribed to the poor sampling along the path as well as the non-equilibrium character of a fast pulling. Fortunately, both effects can be eliminated and the equilibrium PMF profile can be estimated by means of the Jarzynski equality,[22] as discussed elsewhere.[23]

The associated and dissociated states of the NPs were defined by setting the distance between the NPs at 6 and 10 nm, respectively. The association process started with the NPs held 10 nm away from one another by a harmonic potential with a force constant of 4000 kJ mol^{-1} nm^{-2}. The reference distance was varied at 0.05 nm steps down to 6 nm, resulting in 80 sampling windows. At each window, an MD simulation was performed for 2 ns before changing the reference distance again. Once the associated state was reached at 6 nm, the direction of sampling was reversed. This cycle was repeated five times, resulting in a set of raw distribution data, from which the unbiased PMF profiles may be extracted using the weighted histogram analysis method (WHAM).[24] The resulting PMF curves were averaged at each position along the path by means of the Jarzynski equality (eqn (2)):[22,23]

$$\mathrm{PMF}(r) = -RT\left[\frac{1}{n}\sum_{i=1}^{n}\exp\left(-\frac{\mathrm{PMF}_i(r)}{RT}\right)\right] \qquad (2)$$

This average assumes that all replicas share the same reference state, which we have chosen to be the farthest separation between the NPs and have set the PMF to zero at this separation, *i.e.*, PMF(10 nm) = 0 kJ mol^{-1}. Using this reference state, the average PMF at any position along the path is an estimate for the reversible work to bring the two NPs from the reference, dissociated state to position r. In particular, for the position of minimum along the profile, PMF($r_{\min}$) = Δ_{ag}G, where Δ_{ag}G stands for the Gibbs energy of aggregation for a pair of NPs.

The Gibbs energy may be split into its enthalpic and entropic contributions using the standard thermodynamic result (eqn (3)):

$$\Delta_{ag}G = \Delta_{ag}H - T\Delta_{ag}S \qquad (3)$$

In practice, we performed the PMF calculations at five different temperatures (290, 295, 300, 305 and 310 K) and assumed that Δ_{ag}H and Δ_{ag}S should remain nearly constant at this narrow temperature range, and then computed these contributions straightforwardly by the linear regression of Δ_{ag}G values as a function of the temperature.

Results and discussion

Spontaneous self-assembling in chloroform

The final lattice spacing, defined as the position of the minimum after the first correlation peak in the radial distribution function, between the NPs center of mass was found to converge after 500 ns

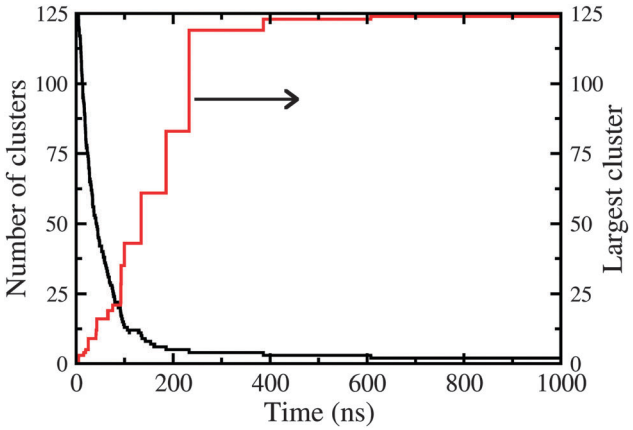

Fig. 3 Time evolution of the number of clusters (black line) and the size of the largest cluster (red line).

to r_{cut} = 7.65 nm. This cut-off distance means that two NPs found at distances with $r \leq r_{cut}$ should be regarded as belonging to the same cluster. This geometrical criterion allowed the calculation of the number of clusters (N) and the size of the largest NP cluster (N_{max}) along the simulation (Fig. 3). At the beginning of the simulation, all NPs were farther than r_{cut} from each other, so only monomers were observed during the first few nanoseconds (N = 125 and N_{max} = 1). The initial evolution of the system may be regarded as a Brownian dynamics process, since the NP separation is large as compared to the interaction cut-off and initial velocities were randomly assigned. After a few nanoseconds, collisions between NPs were observed and most of them resulted in the formation of stable aggregates. As a general trend, the collisions between monomers formed dimers, which in turn collided to form larger and more complex aggregates and so on, until *ca.* 600 ns, when all but one NP formed a single cluster (N = 2 and N_{max} = 124). The only NP that remained free in solution seemed to be stable in this state, since we observed it diffusing away for hundreds of nanoseconds without any structural or energetic indication that it might get incorporated into the large aggregate.

A purely geometrical criterion would suffice for a hard sphere model, for instance, but the NPs always bear a soft organic layer on their surfaces, which may relax slowly during the aggregation process. This structural reorganization was assessed by means of the intermolecular potential energy profiles along the simulation (results not shown here). NP–NP interaction became more attractive as the aggregation proceeded, until *ca.* 700 ns, when it levels off. This is the timescale for the relaxation of NP–solvent and solvent–solvent interactions as well, confirming that, following collisions between two NPs, there is a time lag during which structural reorganization takes place. Energy partitioning yields an interesting picture of the overall self-assembling process: *ca.* −2100 kJ mol^{-1} per NP is the amount of stabilization energy due to the increase in contact area between NPs, along with *ca.* 2900 kJ mol^{-1} per NP of destabilization energy arising from the smaller exposure of NPs to surrounding solvent. Released solvent molecules become incorporated into surrounding bulk solvent and this process contributed with *ca.* −1400 kJ mol^{-1} per NP of

stabilization energy to result in an overall stabilization of *ca.* −600 kJ mol^{-1} per NP. This figure is much larger than the average thermal energy at 300 K, which means that the observed self-assembling must be regarded as an irreversible process.

The slow energy relaxation after 600 ns should be associated with the structural rearrangements of the NPs comprising the cluster. Comparison between the radial distribution of NPs at two blocks of the main trajectory, one from 500 to 600 ns and the other from 900 to 1000 ns, presented a subtle increase in the first correlation peak centered at 6.5 nm and a larger increase in the second and third peaks, centered at 10.8 and 13.0 nm, respectively (Fig. 4). These changes in the correlation profile may also be presented as the change in coordination numbers, which increased in the first coordination shell from 6.5 NPs between 500 and 600 ns to 7.3 NPs between 900 and 1000 ns. Larger changes in coordination numbers have also been observed for the second and third correlation peaks, which is consistent with the slow diffusion and reorganization of NPs inside the cluster after the collisions that led them to self-assemble.

One word of caution may be necessary here, regarding the atypical radial distribution profiles. As compared to homogeneous systems, any systems with some degree of phase separation tend to produce distributions with correlation peaks of large intensity, due to the stable aggregation of the structural unities at short distances. Also, we have not observed the typical plateau of isotropic distribution ($g(r) = 1$), indicating that our model system is not large enough to capture the long-range structure of this heterogeneous system.

The final structure after 1 μs of integration of the equations of motion presented a continuous pattern of threads (Fig. 5) similar to those observed for several nanostructured systems.[25–28] Although the major thread interacts with its periodic images along the *z*-direction, forming one single superstructure in that direction, this long-range pattern may be a finite size effect of the model and should not be regarded as a reliable structural feature until simulations using larger model systems become available. Keeping our focus on the local structure, the main feature arising from the model system is the presence of interconnected threads with 2–4 NPs in diameter. This structure was obtained in the presence of chloroform as the solvent, but it must be clearly stated that the mole fraction of NPs in the model system is much larger than the usual concentrations for the colloidal suspensions studied experimentally. On one hand, this difference in composition renders the results inadequate to describe a dilute suspension. On the other, the model system should be closer to the drying solution over a carbon grid just before the TEM imaging.

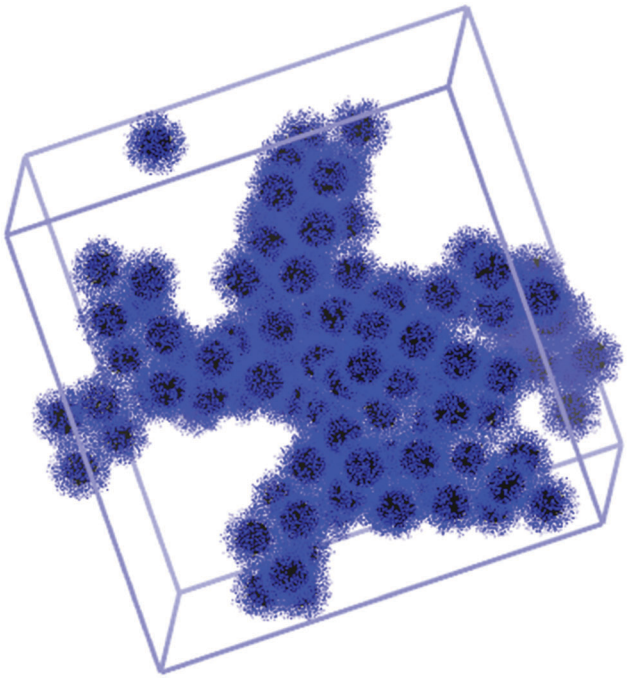

Fig. 5 Structure of the NPs after 1000 ns (solvent molecules are not shown for clarity).

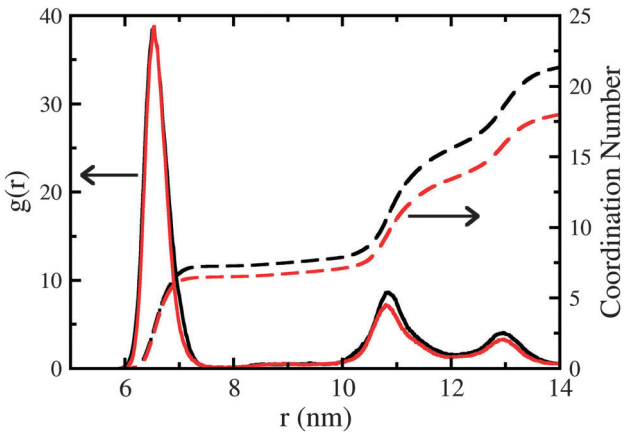

Fig. 4 Radial distribution functions (solid lines) and coordination numbers (dashed lines) for the center of mass of the NPs. The black lines stand for correlation between 900 and 1000 ns, whereas the red lines stand for the correlations between 500 and 600 ns.

NP deposition on a graphene surface and TEM

Although the large concentration of NPs should make our model suspension similar to a drying suspension on a typical TEM grid, we cannot take for granted the correspondence between the structural features appearing in Fig. 5 and the experimental TEM images. The most serious drawback in this kind of comparison is the fact that simulation produced a 3D structure whereas TEM and other imaging techniques usually yield 2D patterns. In order to improve the comparison between model and experiment we carried out the transfer of the equilibrated suspension from the bulk model to a solid substrate in a large, evacuated model.

The cubic box taken from the last point of the bulk simulation readily formed a spherical droplet in equilibrium with chloroform vapor (Fig. 6a and b). The external force employed to pull the droplet in the *z*-direction was turned off as soon as the liquid touched the solid substrate (Fig. 6c) and thereafter only the interfacial forces were responsible for the evolution of the system (this was also the point when the solvent removal was activated). The droplet spontaneously collapsed into a liquid layer of *ca.* 15 nm of thickness over the graphene substrate (Fig. 6d and e).

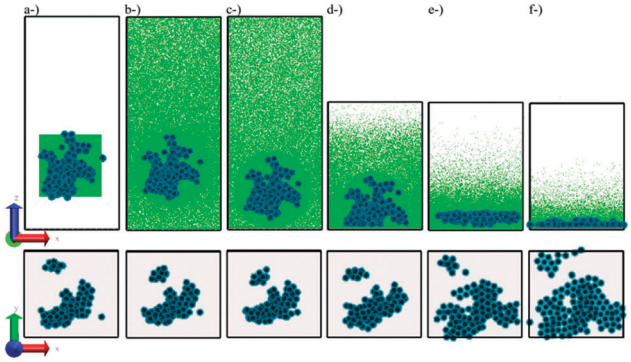

Fig. 6 Graphical representations of selected structures along the relaxation of the liquid suspension droplet and the drying process of the solvent. Solvent molecules are rendered in green in the top view, along with nanoparticles (blue) and the solid substrates (silver). The bottom representations omit the solvent for clarity and present the nanoparticles rendered as solids spheres (solid core) surrounded by a shaded area (capping organic ligands). (a) Final structure obtained from the bulk simulation placed in the middle of the larger box; (b) droplet relaxation and initial solvent evaporation; (c) first contact of the droplet with the substrate and the starting point for the drying process; (d) intermediate point of droplet spreading over the substrate; (e) complete spreading of the liquid suspension; (f) removal of most of the solvent. The edge length of the simulation box in the z-direction was decreased after the start of the drying process in order to improve the computational efficiency.

It is interesting to note that most of the reorganization of NPs took place while the droplet spread over the substrate.

Interfacial tension should be regarded as the driving force for the spreading and the resulting deformation of the liquid produced a dragging force on the NPs, which was strong enough to flatten the 3D aggregate into a 2D version of itself but was not strong enough to change the main structural features which were already present in the bulk solution (Fig. 5).

NPs tended to accumulate at the liquid/vapor interface during the formation of the liquid film, reducing the solvent exposed area and consequently the rate of spontaneous vaporization of chloroform molecules. The number of solvent molecules already in the gas phase became very small and the overall performance of the drying process decreased, and thus after 50 ns we had to change the protocol in order to accelerate the solvent removal rate. Regarding the removal of the vapor above the liquid, we removed all solvent molecules with z-coordinates larger than 50 nm every 0.1 ns, instead of the previous cutoff of 90 nm. And besides removing vaporized molecules, we introduced an extra removal step every 1.0 ns, which consisted of deleting 4000 randomly chosen solvent molecules, regardless of their location in the system. This new removal protocol, although less realistic than that originally proposed, should not introduce significant changes in the NP arrangement, since the NP aggregation should be stabilized with a decreased amount of solvent molecules, as discussed below. Altogether, the drying protocol took 170 ns to remove all solvent, followed by 1.5 ns of MD simulation for the dry NPs over the graphene substrate to allow the structural relaxation of the aggregates.

The average distance between the center of mass of the NPs decreased from 6.45 nm to 6.15 nm during the final stages of the drying process, forming a progressively more compact arrangement (Fig. 6e and f), which remained stable after the complete removal of the solvent (Fig. 7). Readers are referred to the ESI† to watch the movies depicting the details of the drying process.

The comparison between TEM results and the final structure of the thin film simulation is remarkable, with the same structural features appearing in both representations (Fig. 7). Among other patterns, both TEM and simulation agreed that

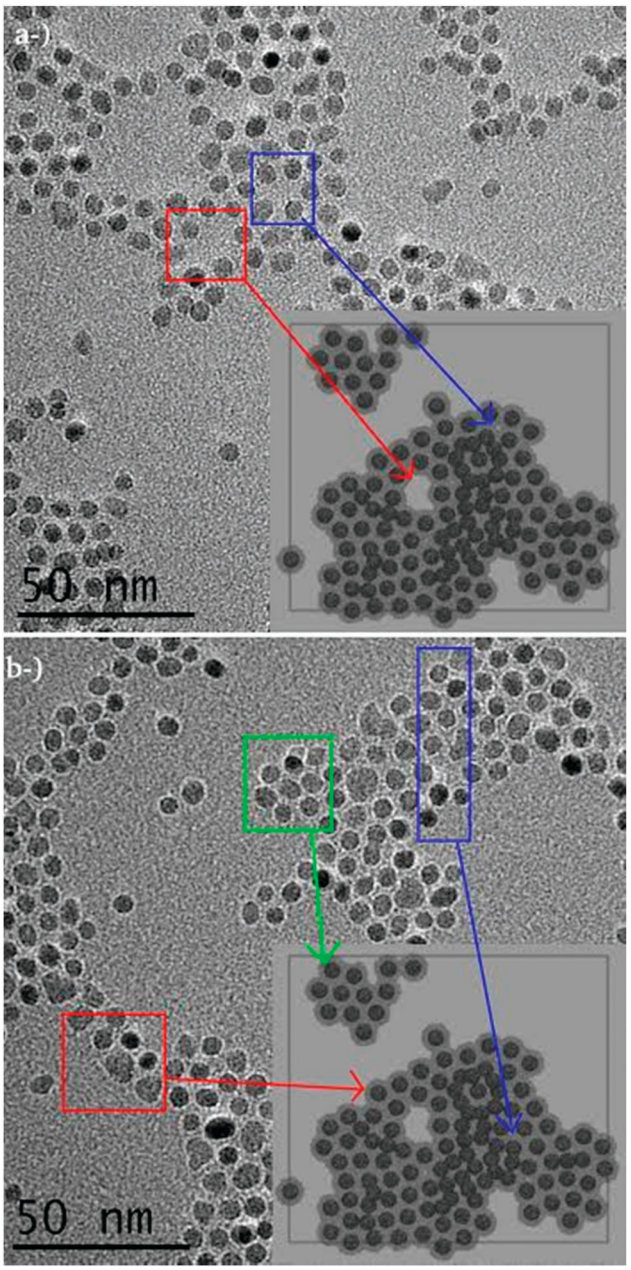

Fig. 7 Comparison between the TEM analysis (larger background images) and the final structure obtained in the thin film simulation (smaller inset images), highlighting similar patterns (all images are drawn on the same scale). (a) Holes in the main structure; and (b) filaments of similar size and shape. Simulation images depict the NPs cores as solid spheres and the organic capping as shaded areas around the cores.

thin films presented a hexagonal packing and form 2D thread-like structures with holes of varying size and a few protrusions outside the main filaments. Altogether, this remarkable agreement lends support to our modeling strategy, including both the choice of the coarse grained model and the protocols that we have devised for the deposition of the suspension droplet and for the solvent removal.

Gibbs energy of aggregation

The equilibrium molecular dynamics simulations for the NPs either in chloroform suspension or on the surface of a solid substrate without any solvent are consistent with the spontaneous self-assembling of the NPs to form large and stable aggregates. The thermodynamic potentials driving these association processes may be conveniently assessed by means of umbrella sampling simulations for a pair of NPs either in chloroform or in a vacuum.

Ten independent replicas of the potential of mean force were computed for the NP pair in chloroform, five replicas for the association process and five for the dissociation process (Fig. 8). The profiles for the association process presented a larger dispersion as compared to the profiles for the dissociation process, but this difference between the two processes, although related to the insufficient sampling of each individual profile, should not be taken as a sign for hysteresis before the profiles are properly averaged. This averaging may be conveniently performed using the Jarzysnki equality at each position along the reaction coordinate. The averages for the two processes are nearly identical along most of the profiles, except for two regions, one from 6.5 to 7.0 nm and the other from 8.0 to 8.5 nm (Fig. 8), where small hysteresis were observed. These differences may be ascribed either to the reorganization of the oleic acid tails or to the solvation–desolvation processes, respectively, and they may be safely regarded as small hysteresis since they amount to less than the average thermal energy. As long as only a minor overall hysteresis was observed, both association and dissociation profiles may be combined into a single Jarzynski average. The resulting profile varies smoothly and there are neither activation barriers nor local minima along the pathway from the separated monomers to the dimer in solution (Fig. 8).

The choice of the monomers separated by 10.0 nm as the reference state was made in advance and the average profile confirmed that it was an adequate choice, since the average potential of mean force leveled off to a stable plateau between 8.0 and 10.0 nm for all temperatures but T = 310 K, which presented a small activation barrier between the monomeric state and the aggregated state (Fig. 9). The barrier height is smaller than the average thermal energy and thus it should not induce any degree of kinetic stability that might prevent the self-assembling. Taking the same reference state for all temperatures, the Gibbs energy of aggregation was computed for the NP pair in chloroform at five different temperatures (Fig. 10). The linear regression yielded estimates of -219 kJ mol^{-1} for the aggregation enthalpy and -590 J K^{-1} mol^{-1} for the aggregation entropy (R^2 = 0.908). The unfavorable entropy comes partly from the change in the rotational state of the NPs,[29] which amounts to $R\ln(r/r_0)$, where the reference distance was taken to be r_0 = 10 nm.

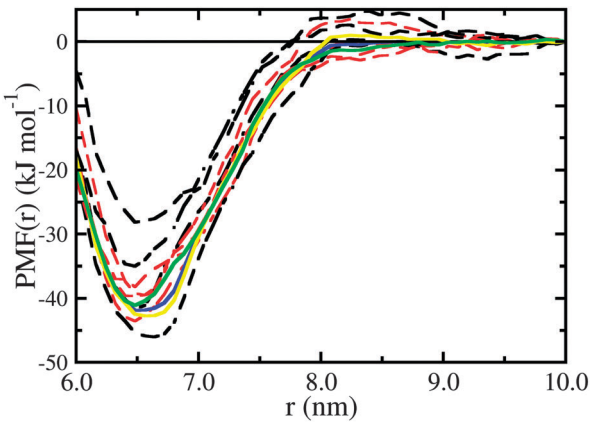

Fig. 8 Work profiles for the association (dashed black curves) and the dissociation (dashed red curves) of a pair of NPs in chloroform. Solid lines stand for the Jarzynski average of the association processes (yellow curve), the dissociation processes (green curve) and the overall average (blue curve).

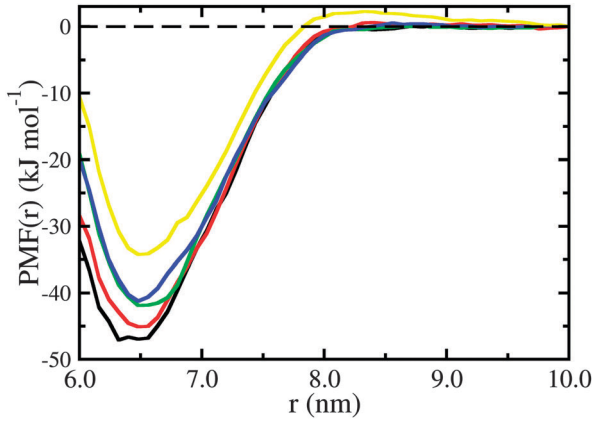

Fig. 9 Jarzynski average for the PMF along the association/dissociation profile for a pair of NPs in chloroform at different temperatures. (black line) 290 K; (red line) 295 K; (green line) 300 K; (blue line) 305 K; (yellow line) 310 K.

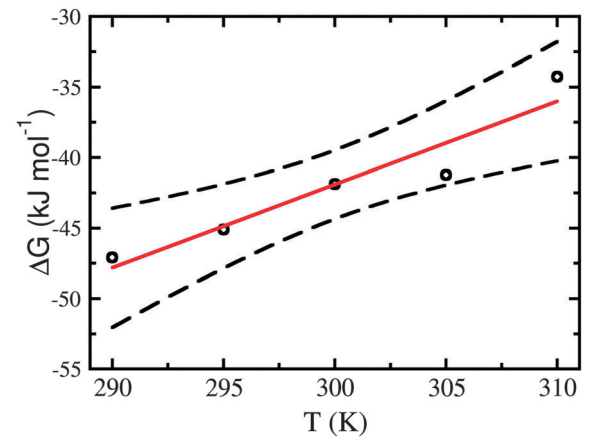

Fig. 10 Gibbs energy of aggregation for a pair of NPs in chloroform. The solid red line stands for the linear regression whereas the dashed black lines stand for the confidence interval of the regression.

Although this is a small contribution as compared to the overall entropy change, amounting to only -3.6 J K^{-1} mol^{-1}, it causes the Gibbs energy to increase by *ca.* 1 kJ mol^{-1} at 300 K.

The same procedure was repeated for the NP pair in a vacuum, resulting in a set of steeper profiles for the averaged PMF (Fig. 11). The first thing to note is the presence of larger hysteresis for all temperatures that were considered, with PMF wells for the dissociation processes lying typically 100 kJ mol^{-1} deeper with respect to the association processes (results not shown here). From the standpoint of the Jarzynski average (eqn (2)), this difference is much larger than RT, meaning that average profiles in Fig. 11 are biased toward the more negative dissociation profiles. Although this might seem to lend the averaged curves unreliable, the difference between the PMF profiles in a vacuum with respect to those in chloroform is so large that some general conclusions should hold even for this biased set of vacuum results. The two relevant results here are the shorter contact position in a vacuum, which is *ca.* 1.5 nm smaller than in chloroform, and the larger thermodynamic stability of the associated NPs in a vacuum as compared to the system with chloroform.

The shorter contact position is consistent with a more compact organic layer on the NP surface for the vacuum simulations. This structural difference may be assessed by the inspection of the cross section view of the NP pair at contact in either chloroform or a vacuum (Fig. 12). Both structures were taken from the last point of one of the umbrella sampling simulations at 300 K, setting r = 5.0 nm for the simulation in a vacuum and r = 6.5 nm for the simulation in chloroform. The organic layer is clearly solvent-swollen in the latter case and shrunk in the former.

The Gibbs energy of aggregation changed from less than 50 kJ mol^{-1} in chloroform (Fig. 9 and 10) to more than 500 kJ mol^{-1} in a vacuum (Fig. 11 and 13) in the temperature range under investigation, which is a clear indication of the destabilization role played by the solvent. The linear regression of the Gibbs energy values yielded an estimate of -2550 kJ mol^{-1} for the aggregation enthalpy and of -6160 J K^{-1} mol^{-1} for the aggregation entropy (R^2 = 0.994). These figures are tenfold larger than those obtained for the Gibbs energy of aggregation in chloroform and this is why we have considered that our *ad hoc* procedure to remove the solvent molecules during the drying of

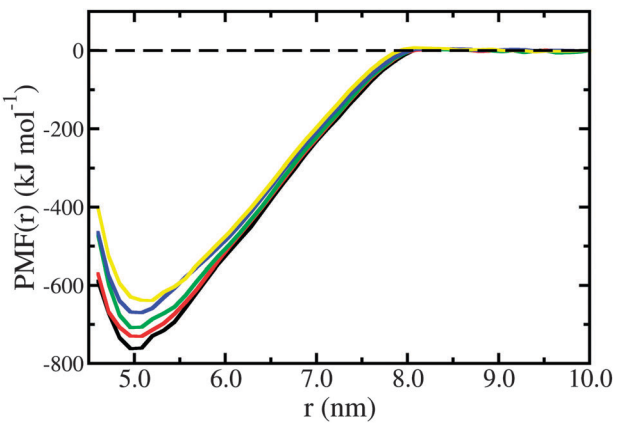

Fig. 11 Jarzynski average for the PMF along the association/dissociation profile for a pair of NPs in a vacuum at different temperatures. (black line) 290 K; (red line) 295 K; (green line) 300 K; (blue line) 305 K; (yellow line) 310 K.

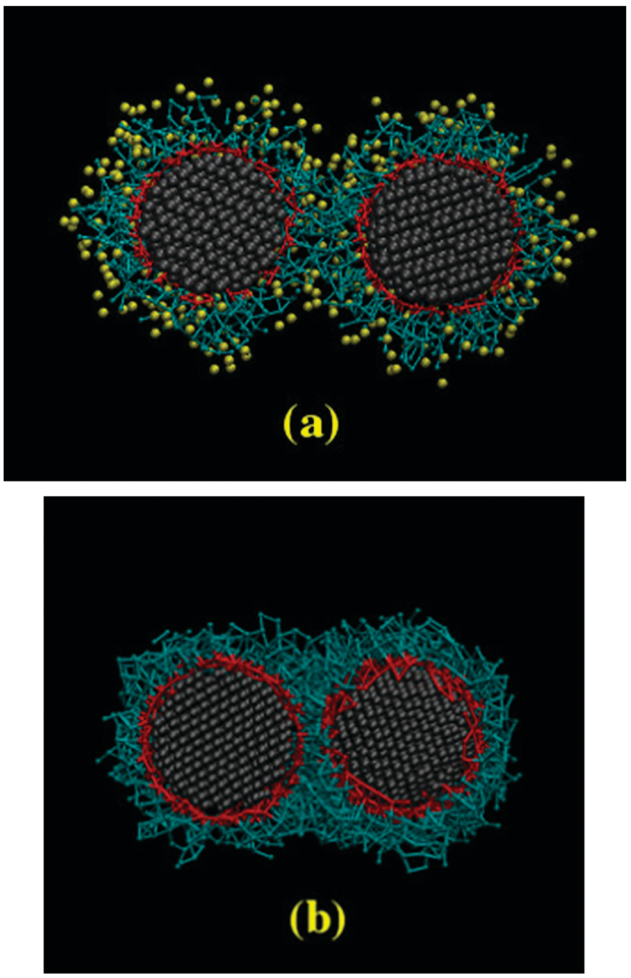

Fig. 12 Cross section view of the NP pair at the distance of minimum Gibbs energy along the PMF profile (T = 300 K) in chloroform (a) and in a vacuum (b). Solvent molecules within 0.5 nm of any NP site are shown in yellow at (a).

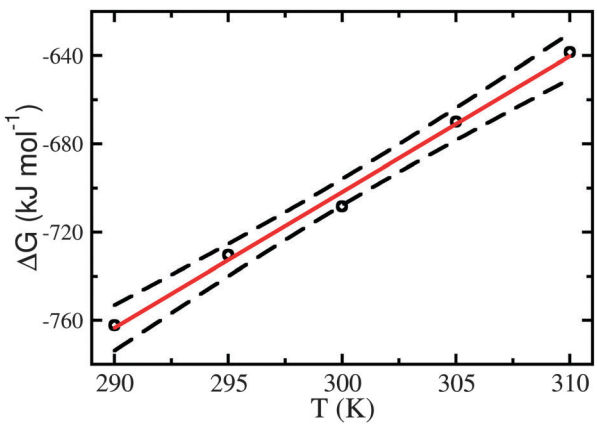

Fig. 13 Gibbs energy of aggregation for a pair of NPs in a vacuum. The solid red line stands for the linear regression whereas the dashed black lines stand for the confidence interval of the regression.

the suspension on the solid substrate should not affect the structure. As a matter of fact, removing the solvent increased the interaction between NPs and rendered the structures more stable than they were in suspension. As regards the enthalpy contribution, the large difference can be easily rationalized by considering the fact that in chloroform the energy contributions tend to cancel out, whereas in a vacuum the NPs change from no interaction for the fully dissociated state to an optimal aggregated state at the minimum PMF.

Although PMF calculations describe the association of a single pair of NPs our large-scale model contained 125 NPs, we must acknowledge the fact that any spontaneous collision during the evolution of the system must be subject to these large thermodynamic potentials driving the NPs to form stable aggregates.

It is interesting to note that considering the potential energy contribution alone is not enough to explain the minimum PMF at $r = 5.0$ nm for the NPs in a vacuum, since the potential energy became steadily more negative as the separation changed from 10 to 4 nm, without showing any sign of leveling off. The well-defined and reproducible minima must then be ascribed to the decrease in entropy as the NPs become aggregated. Besides the rotational entropy decrease of the dimer,[29] each NP could rotate freely around its center of mass prior to the aggregation, but rotation should become progressively hindered as the NPs approach each other. Unfortunately, the PMF contribution arising from this change in the rotational state of each NP around its center of mass is not amenable to any simple, analytic expression.

The unfavourable entropic contribution might seem to be at odds with experimental observations for superlattice formation[30] and theoretical predictions for close-packing of binary hard sphere systems.[31] Nonetheless, Schapotschnikow *et al.*[32] reported PMF profiles for the aggregation of capped gold NPs in a vacuum at three different temperatures and the estimated Gibbs energy of aggregation for these dimers became less negative with temperature increase. Unfortunately, their results could not be used to estimate the magnitude of the unfavourable entropic contribution due to the small number of temperature points and the wide temperature range, which resulted in a non-linear variation for the Gibbs energy. Although qualitative, these findings may be used to further validate our model system, since Schapotschnikow *et al.*[32] used a fully atomistic model and they observed the same trends produced by our coarse grained approach. Besides performing vacuum simulations, they also reported the aggregation of a dimer in hexane and the PMF profile became repulsive at all separations, consistent with our findings on the destabilization of the dimer in chloroform as compared with vacuum. The effect of hexane is larger than that of chloroform mostly because hexane is a better solvent for aliphatic chains.[14] Another computational study by Patel and Egorov[33] provided evidence that the destabilizing effect of a good solvent on the aggregation of capped NPs may be switched on by increasing the solvent density, reinforcing the idea that solvent-swelled capping layers decrease the stability of the aggregated state. Temperature may also switch entropic interactions on if the melting point of the chains at the NPs surface is crossed, giving rise to steric hindrance between the molten chains.[34] And even in the absence of any attraction contributions between the chains, purely entropic interactions arise from the excluded volume of the chains on the NP surface.[35] These excluded volume interactions may be modulated by the medium composition, ranging from purely repulsive contributions arising from the chains to attractive interactions arising from the depletion of solutes and solvents in the intervening space between NPs.[35]

Conclusions

The most important and general conclusion that may be drawn from the comparison of simulation results and experimental findings is that our modeling strategy should be regarded as reliable. The morphology of the aggregates was in excellent agreement with the structures that were observed experimentally using TEM, giving support to validity of using a simplified model to describe the self-assembling of large and complex systems as long as the interactions of the surface sites are properly described. This finding highlights the fact that the self-assembling and the self-organization of NPs are directed by the competition between different interfacial tension components.

Another general and important conclusion regarding the reliability of the modeling strategy is that the model system size matters when it comes to the proper description of the aggregate morphology. The same system had already been modeled using only eight NPs,[14] which were large enough to correctly predict the stable aggregation of the NPs in chloroform on the one hand, but on the other was not large enough to describe the structural patterns that should arise from the aggregation. This is why we have chosen to increase 15-fold the system size and 5-fold the simulation timescale, and both choices proved to be effective and necessary.

The stabilization energy per NP is much larger than the average thermal energy under ambient conditions, pointing out to an irreversible aggregation. This conclusion is also supported by the Gibbs energy of aggregation, which is much larger than the average thermal energy as well. It should be noted, however, that the entropy of aggregation is unfavorable both in chloroform and in a vacuum, making the temperature an important factor affecting the thermodynamic stability of the aggregates. On the one hand, the increase in temperature to destabilize the aggregates in chloroform would be so large that the solvent would be vaporized long before the entropic term could become dominant. In a vacuum, on the other hand, it would be possible to disrupt the aggregates if the material was heated up to *ca.* 140 °C (assuming constant enthalpy and entropy contributions during heating), a temperature which may be easily reached, allowing in principle to control the aggregation state of the powdered material.

Altogether, our findings and those from previous computer simulations point out to complex roles played by the entropic contributions during NP self-assembling. And most importantly, these contributions may be modulated by changes in composition, pressure and temperature, opening up new perspectives in the control of NP self-assembling and self-organization.

Acknowledgements

This work was partially supported by the Center for Photonic and Multiscale Nanomaterials (C-PHOM) funded by the National Science Foundation (NSF) Materials Research Science and Engineering Center program DMR 1120923; NSF EFRI-ODISSEI: Multi-scale Origami for Novel Photonics, Energy Conversion, NSF-1240264. NSF projects CBET 1036672 and CBET 1403777; the U. S. Army Research Office under Grant Award No. W911NF-10-1-0518; DOD/ASDRE under Award No. N00244-09-1-0062 and AFOSR Grant Award MURI W911NF-12-1-0407. We also acknowledge FAPESP (2012/15147-4), CNPq and CAPES (Brazilian funding agencies) for the financial support.

Notes and references

1 S. Srivastava, A. Santos, K. Critchley, K.-S. Kim, P. Podsiadlo, K. Sun, J. Lee, C. Xu, G. D. Lilly, S. C. Glotzer and N. A. Kotov, *Science*, 2010, **327**, 1355.
2 H. J. C. Berendsen, *Simulating the Physical World: Hierarchical Modeling from Quantum Mechanics to Fluid Dynamics*, Cambridge University Press, Cambridge, 2007.
3 S. W. Cranford, A. Tarakanova, N. M. Pugno and M. J. Buehler, *Nature*, 2012, **482**, 72.
4 A. Baskin, W.-Y. Lo and P. Král, *ACS Nano*, 2012, **7**, 6083.
5 E. Heikkilä, A. A. Gurtovenko, H. Martinez-Seara, H. Häkkinen, I. Vattulainen and J. Akola, *J. Phys. Chem. C*, 2012, **116**, 9805.
6 B. L. Peters, J. M. D. Lane, A. E. Ismail and G. S. Grest, *Langmuir*, 2012, **28**, 17443.
7 J. M. D. Lane and G. S. Grest, *Phys. Rev. Lett.*, 2010, **104**, 235501.
8 J. M. D. Lane and G. S. Grest, *Nanoscale*, 2014, **6**, 5132.
9 C.-K. Lee, C.-W. Pao and C.-W. Chen, *Energy Environ. Sci.*, 2013, **6**, 307.
10 S. Leekumjorn, S. Gullapalli and M. S. Wong, *J. Phys. Chem. B*, 2012, **116**, 13063.
11 S. J. Marrink, H. J. Risselada, S. Yefimov, D. P. Tieleman and A. H. de Vries, *J. Phys. Chem. B*, 2007, **111**, 7812.
12 P. F. Damasceno, M. Engel and S. C. Glotzer, *Science*, 2012, **337**, 453.
13 J.-Q. Lin, H.-W. Zhang, Z. Chen, Y.-Z. Zheng, Z.-Q. Zhang and H.-F. Ye, *J. Phys. Chem. C*, 2011, **115**, 18991.
14 C. J. Dalmaschio, E. G. S. Firmiano, A. N. Pinheiro, D. G. Sobrinho, A. F. de Moura and E. R. Leite, *Nanoscale*, 2013, **5**, 5602.
15 L. Sun, X. Yang, B. Wu and L. Tang, *J. Chem. Phys.*, 2011, **135**, 204703.
16 Z. Yang, X. Yang, Z. Xu and N. Yang, *J. Chem. Phys.*, 2010, **133**, 094702.
17 B. Hess, C. Kutzner, D. van der Spoel and E. Lindahl, *J. Chem. Theory Comput.*, 2008, **4**, 435.
18 D. van der Spoel, E. Lindahl, B. Hess, G. Groenhof, A. E. Mark and H. J. C. Berendsen, *J. Comput. Chem.*, 2005, **26**, 1701.
19 W. Humphrey, A. Dalke and K. Schulten, *J. Mol. Graphics*, 1996, **14**, 33.
20 G. Bussi, D. Donadio and M. Parrinello, *J. Chem. Phys.*, 2007, **126**, 014101.
21 H. J. C. Berendsen, J. P. M. Postma, A. DiNola and J. R. Haak, *J. Chem. Phys.*, 1984, **81**, 3684.
22 C. Jarzynski, *Phys. Rev. Lett.*, 1997, **78**, 2690.
23 K. Bernardino and A. F. de Moura, *J. Phys. Chem. B*, 2013, **117**, 7324.
24 S. Kumar, D. Bouzida, R. H. Swendsen, P. A. Kollman and J. M. Rosenberg, *J. Comput. Chem.*, 1992, **13**, 1011.
25 L. Cademartiri, K. J. M. Bishop, P. W. Snyder and G. A. Ozin, *Philos. Trans. R. Soc., A*, 2012, **370**, 2824.
26 G. Ma, Y. Zhou, X. Li, K. Sun, S. Liu, J. Hu and N. A. Kotov, *ACS Nano*, 2013, **7**, 9010.
27 A. J. Houtepen, R. Koole, D. Vanmaekelbergh, J. Meeldijk and S. G. Hickey, *J. Am. Chem. Soc.*, 2006, **128**, 6792.
28 S. H. Sun, S. Anders, T. Thomson, J. E. E. Baglin, M. F. Toney, H. F. Hamann, C. B. Murray and B. D. Terris, *J. Phys. Chem. B*, 2003, **107**, 5419.
29 R. M. Neumann, *Am. J. Phys.*, 1980, **48**, 354.
30 M. I. Bodnarchuk, M. V. Kovalenko, W. Heiss and D. V. Talapin, *J. Am. Chem. Soc.*, 2010, **132**, 11967.
31 M. D. Eldridge, P. A. Madden and D. Frenkel, *Nature*, 1993, **365**, 35.
32 P. Schapotschnikow, R. Pool and T. J. H. Vlugt, *Nano Lett.*, 2008, **8**, 2930.
33 N. Patel and S. A. Egorov, *J. Chem. Phys.*, 2007, **126**, 054706.
34 A. Widmer-Cooper and P. Geissler, *Nano Lett.*, 2014, **14**, 57.
35 A. Striolo, *Phys. Rev. E: Stat., Nonlinear, Soft Matter Phys.*, 2006, **74**, 041401.